



AMS
American Meteorological Society

Supplemental Material

© Copyright 2024 [American Meteorological Society](https://www.ametsoc.org) (AMS)

For permission to reuse any portion of this work, please contact permissions@ametsoc.org. Any use of material in this work that is determined to be “fair use” under Section 107 of the U.S. Copyright Act (17 USC §107) or that satisfies the conditions specified in Section 108 of the U.S. Copyright Act (17 USC §108) does not require AMS’s permission. Republication, systematic reproduction, posting in electronic form, such as on a website or in a searchable database, or other uses of this material, except as exempted by the above statement, requires written permission or a license from AMS. All AMS journals and monograph publications are registered with the Copyright Clearance Center (<https://www.copyright.com>). Additional details are provided in the AMS Copyright Policy statement, available on the AMS website (<https://www.ametsoc.org/PUBSCopyrightPolicy>).

JOURNAL OF CLIMATE

SUPPLEMENTARY MATERIAL

Non-stationarity in the NAO–Gulf Stream SST front interaction

Luca Famooss Paolini, Nour-Eddine Omrani, Alessio Bellucci,
Panos J. Athanasiadis, Paolo Ruggieri, Casey Patrizio, Noel Keenlyside.

Luca Famooss Paolini

Department of Physics and Astronomy, University of Bologna, Bologna, Italy

luca.famoospaolini@unibo.it

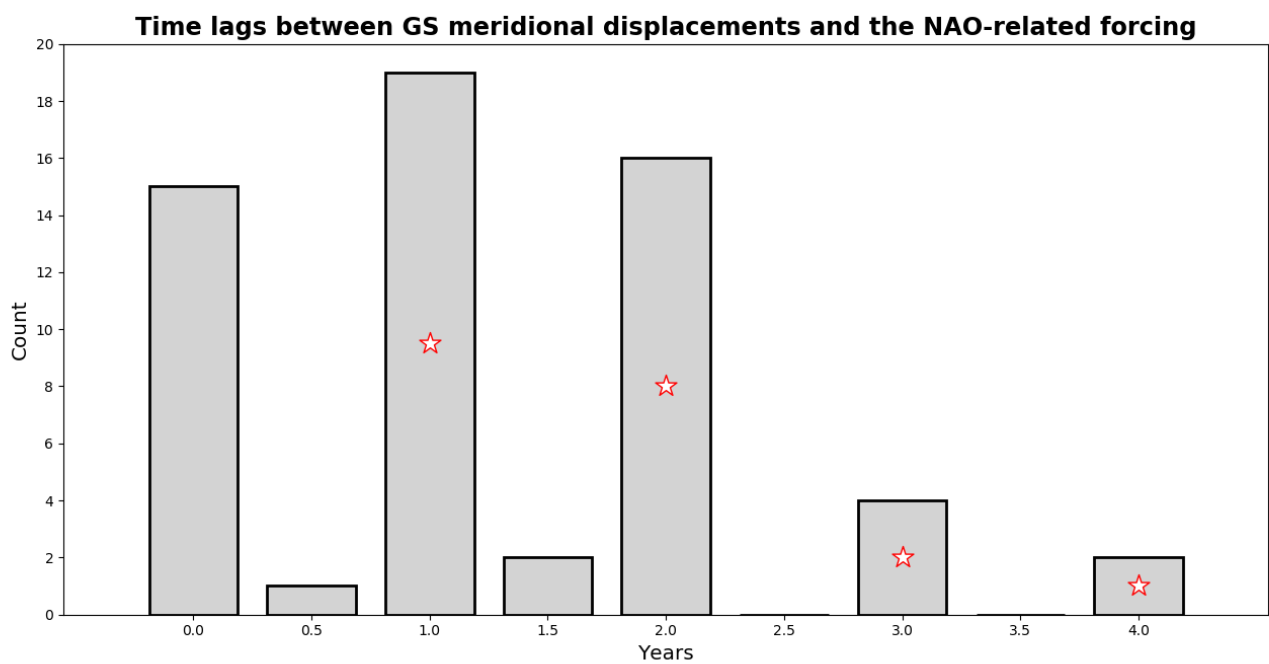


Fig. S1: Histogram of the time lags between Gulf Stream (GS) meridional displacements and the North Atlantic Oscillation (NAO)-related forcing suggested in literature, as reported in Table 1 in the main text. The stars identify the time lags where the correlation between the GS sea surface temperature (SST) front (GSF) and NAO indices is found to be statistically significant at 95% confidence level in the present work.

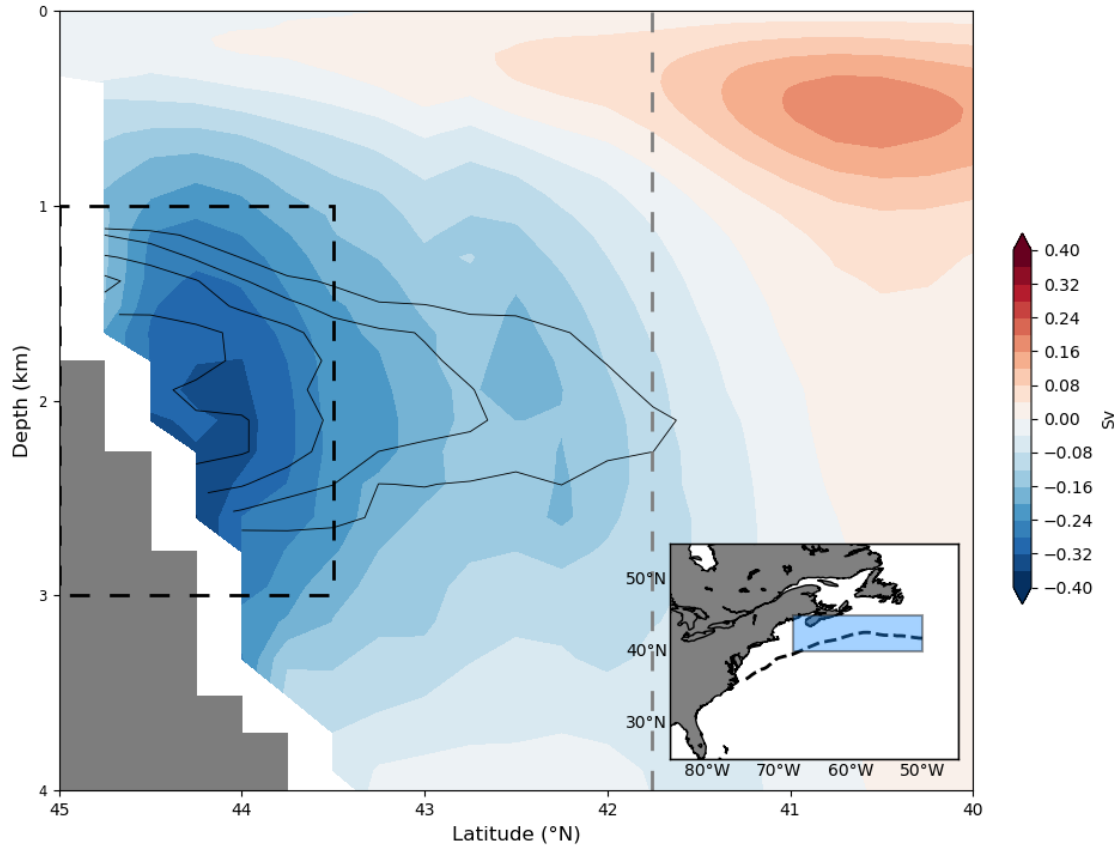


Fig. S2: Latitude–depth cross section of the winter mean zonal transport (Sv ; color shading) in ORAS5 dataset averaged in the 50° – $68^{\circ}W$ longitudinal range. The black contours indicate the winter mean potential vorticity averaged in the 50° – $68^{\circ}W$ longitudinal range every $0.5 \times 10^{-12} \text{ m}^{-1} \text{ s}^{-1}$ from $2.5 \times 10^{-12} \text{ m}^{-1} \text{ s}^{-1}$. It is specified that the potential vorticity is lower close to the coast and it increases towards the open sea. The vertical dashed line represents the GSF latitudinal position averaged in the 50° – $68^{\circ}W$ longitudinal range during the winter season. The black dashed box represents the area where the zonal transport has been integrated to define the deep western boundary current (DWBC) index (43.5° – $45^{\circ}N$; 1000–3000 m). For the DWBC index, the sign of the zonal transport has been reversed in order to have positive (negative) DWBC index for anomalous westward (eastward) flow. The blue box in the bottom–right inset shows where the zonal transport, the potential vorticity and the GSF latitudinal position have been averaged along the longitudinal direction (50° – $68^{\circ}W$). The black dashed line in the inset indicates the winter climatological position of the GSF.

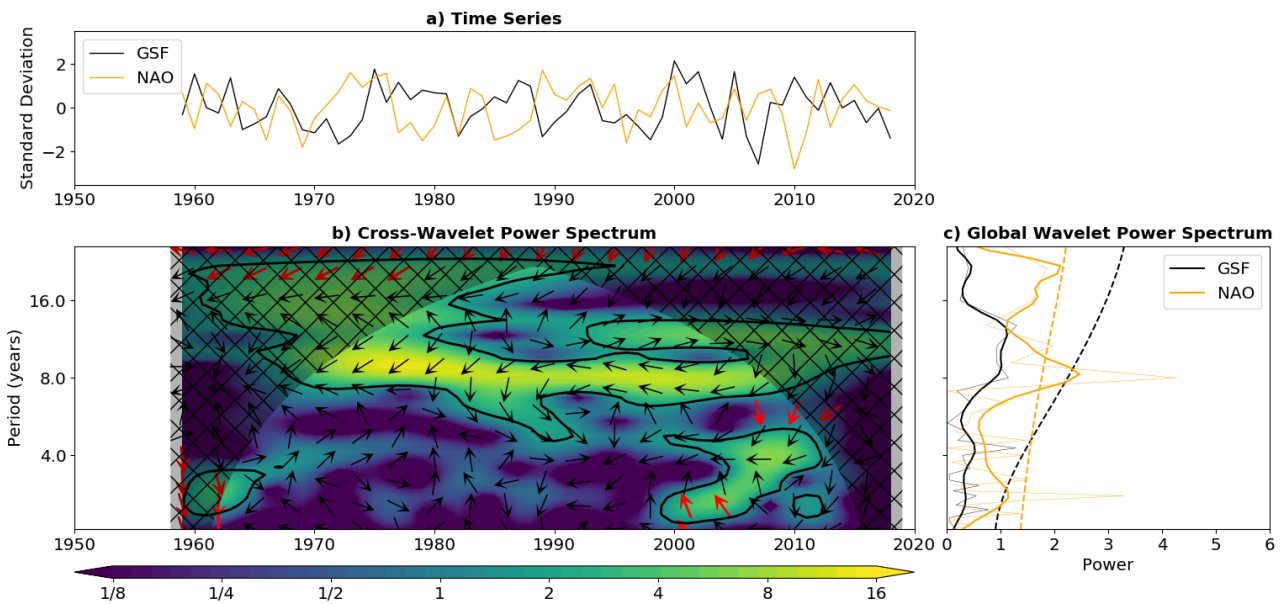


Fig. S3: a) Detrended and standardized winter GSF (black) and NAO (orange) time series in ORAS5 dataset (1958–2018). b) Cross-wavelet transform of the winter GSF and NAO time series. Thick black contours enclose cross-wavelet power spectrum statistically significant at 90% confidence level. Phase relationship between the winter GSF and NAO time series is shown as vectors, following the convention in Torrence and Webster (1999). In case of in-phase signals, vectors point upwards; in case of anti-phase signals, vectors point downwards. If the GSF leads the NAO, vectors point to the right; if the NAO leads the GSF, vectors point to the left. Thick red vectors indicate phase relationship where squared wavelet coherence is statistically significant at 90% confidence level (Kohyama et al., 2021). Cross-hatched light shades indicate the cone of influence, where edge effects may alter the power spectrum. c) Global wavelet (bold) and Fourier (thin) power spectrum of detrended and standardized winter GSF (black) and NAO (orange) time series. The bold dashed lines represent the 90% confidence level of time-averaged red- (black) and white-noise (orange) spectra. The x-axis range in a) and b) is 1950–2020, in order to be comparable with the ERA5 reanalysis dataset (Figure 1).

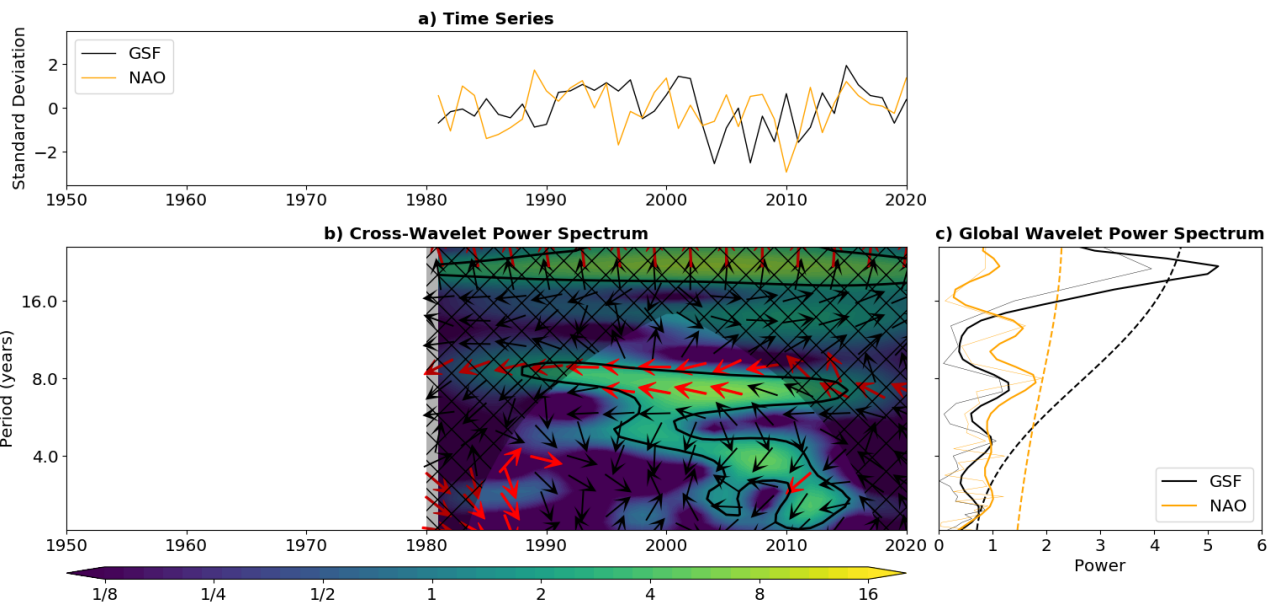


Fig. S4: Same as Figure S3 but in SODA3.4.2 dataset (1980–2020).

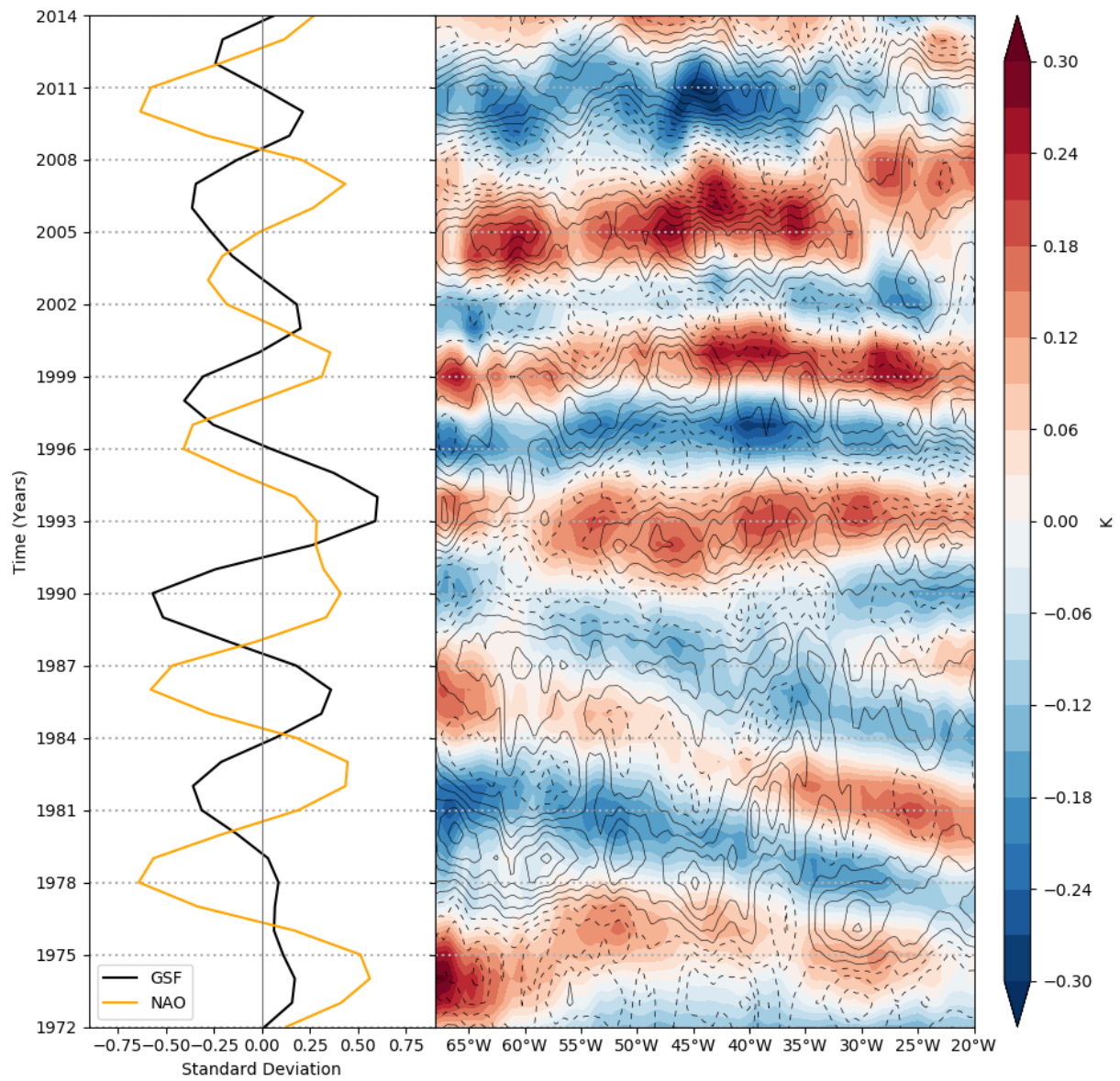


Fig. S5: Left panel: Band-pass filtered winter GSF (black) and NAO (orange) time series between 1972–2014. Right panel: Hovmöller diagram of the band-pass filtered SST (K; color shading) and wind-stress curl anomalies (10^{-7} N m^{-3} ; black contours; contours every $0.1 \times 10^{-7} \text{ N m}^{-3}$ from $-1 \times 10^{-7} \text{ N m}^{-3}$) averaged in the 35° – 38°N and 35° – 37°N latitudinal range during 1972–2014, respectively. It is specified that 6 years are lost at each border of the time series because of the application of the Lanczos filter (see detail in section 2 in the main text). For this reason, the y-axis of the plot ranges from 1972 up to 2014 and not from 1972 up to 2018, that is when the GSF and NAO covary at the decadal timescale (Figure 1).

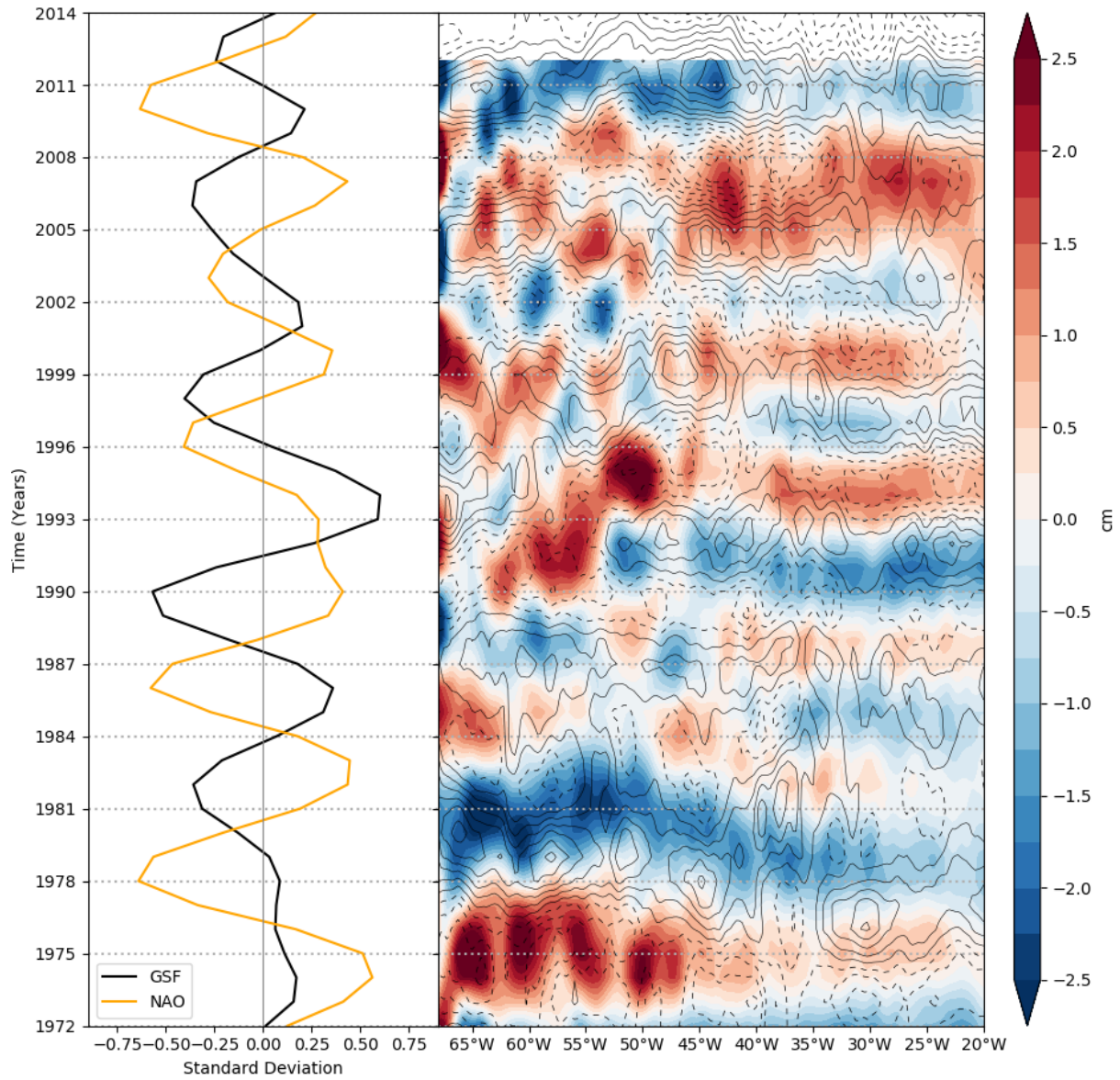


Fig. S6: Same as Figure S5 but for the band-pass filtered sea surface height (SSH; cm; color shading) and wind-stress curl anomalies (10^{-7} N m^{-3} ; black contours; contours every $0.1 \times 10^{-7} \text{ N m}^{-3}$ from $-1 \times 10^{-7} \text{ N m}^{-3}$).

References

Kohyama, T., Yamagami, Y., Miura, H., Kido, S., Tatebe, H., and Watanabe, M. (2021). The Gulf Stream and Kuroshio Current are synchronized. *Science*. Publisher: American Association for the Advancement of Science.

Torrence, C. and Webster, P. J. (1999). Interdecadal Changes in the ENSO–Monsoon System. *Journal of Climate*, 12(8):2679–2690. Publisher: American Meteorological Society Section: Journal of Climate.